IOPscience iopscience.iop.org

Home Search Collections Journals About Contact us My IOPscience

Structural and electron transport properties of Mo/Al multilayer films

This article has been downloaded from IOPscience. Please scroll down to see the full text article.

1990 J. Phys.: Condens. Matter 2 1179

(http://iopscience.iop.org/0953-8984/2/5/011)

View the table of contents for this issue, or go to the journal homepage for more

Download details:
IP Address: 171.66.16.96
The article was downloaded on 10/05/2010 at 21:37

Please note that terms and conditions apply.

J. Phys.: Condens. Matter 2 (1990) 1179–1195. Printed in the UK

Structural and electron transport properties of Mo/Al multilayer films

T Izumiya, T Hanamure, E Saito, T Kaneko and R Yamamoto
Department of Materials Science, Faculty of Engineering, University of Tokyo, Bunkyo-ku, Tokyo 113, Japan

Received 13 April 1989, in final form 12 September 1989

Abstract. Metallic Mo/Al multilayers have been successfully fabricated by a magnetron–radiofrequency sputtering system. The modulation wavelength ranged from 640 down to 15 Å. Detailed structural properties were studied using x-ray and electron diffraction methods. These studies indicated that the films are polycrystalline with high structural order, BCC Mo (1 1 0) and FCC Al (1 1 1) parallel to the films. Model calculations based on paracrystal theory were performed to analyse the x-ray diffraction patterns. In-plane resistivity was measured as a function of the modulation wavelength and temperature. The resistivity did not saturate even at very small wavelength and negative temperature gradients were usual below 60 Å, where enhancements of the superconducting transition temperature were observed.

1. Introduction

Currently, extensive interest has been aroused by observations of enhanced elastic and reduced magnetic properties of short-wavelength compositionally modulated metallic multilayer films (CMF), since these films are capable of initiating the development of new materials not found in nature. Their unique elastic, superconducting, magnetic or x-ray dispersing properties are due to the novel atomic arrangement. A number of bimetallic multilayer films composed of two structurally, physically and chemically dissimilar metals have been synthesised in the last decade. Quite a few researchers have studied the Cu/Ni system, but they have rarely referred to the possibility of the structural order being different in each sample, especially in the measurements of their magnetic moment (Thaler *et al* 1978, Gyorgy *et al* 1983, Zheng *et al* 1981a, 1982, Flevaris *et al* 1982). We should not discuss or compare these properties without referring to their structures, because the structures of the individual layers and interfaces play a key role in the physical properties of these films.

The behaviours for long wavelengths do not significantly differ from that for the bulk materials in contact. As for the structure, it is generally known that with decreasing wavelength coherency strains throughout the film appear instead of mismatch dislocations. For example, Cu/Ni (Gyorgy *et al* 1982) is regarded as a coherent structure and Nb/Cu (Lowe *et al* 1981) as an incoherent one, but this distinction is not clear in metallic CMF systems. The obscurity is due to the fact that they are more or less polycrystalline

films. It is most interesting now to decide whether the difference in the states, coherent or incoherent, or intermediate state, does affect properties of a CMF in a significant way.

The first transport properties of CMF were reported for Cu/Ni (Schuller *et al* 1979). Since then, a few systems, such as Nb/Ti (Zheng *et al* 1981b, Qian *et al* 1982), Nb/Cu (Banerjee *et al* 1982, Bannerjee and Schuller 1984), Nb/Al (Gurvitch 1986), Mo/Ni (Uher *et al* 1984, Clarke *et al* 1985), Pd/Au, Fe/Cr (Shiroishi *et al* 1987), Nb/Zr (Lowe and Geball 1984) and Mo/Cu (Sasaki *et al* 1988, Kaneko *et al* 1988), have been studied, and saturation of resistivity with decreasing wavelength and negative temperature coefficient of resistivity (TCR) were observed. The saturation and negative TCR are not necessarily decisive because of the critical wavelengths being so small that appropriate films cannot be prepared satisfactorily in the metallic systems. Furthermore, in Pd/Au (Carcia and Suna 1983), Pd/Co (Carcia *et al* 1985) and Ag/Co (Slaughter *et al* 1987) the resistivities are always not so high as in single-component films and no plateau in the inverse-wavelength dependence of the resistivity was observed. The resistivity of Al/Ge (Haywood and Ast 1978) seems to keep on increasing upon decreasing the wavelength. The question is whether this saturation or negative TCR occurs or not, and whether it has a correlation with the coherency change.

In the present paper we report fabrication of Mo/Al CMF by conventional simple sputtering apparatus. Molybdenum and aluminium are quite dissimilar metals. The former has a BCC lattice and extremely high melting point, whereas the latter has a FCC lattice with a comparatively low melting point. Though their crystal structures are quite different, the atomic densities of the most dense planes are approximately equal. Therefore we can expect a coherent structure. First, the structure of the films was studied by x-ray and electron diffraction methods, and x-ray diffraction patterns were simulated. The electron transport properties were measured and negative TCR were confirmed. We also tried to calculate the resistivities according to the theory of Dimmich (1985) in order to explain the relatively high resistivities in the short-wavelength region. Additionally, an increase of the superconducting temperature was observed in the short-wavelength region.

2. Experimental details

The compositionally modulated Mo/Al films used in this study have average Al concentrations of 25, 50 and 75 at.% with wavelengths ranging between 15 and 640 Å. For x-ray diffraction studies 25% samples were inadequate.

All the samples used in these studies were prepared by radiofrequency (RF) magnetron sputtering in a vacuum system with an oil diffusion pump and a rotating substrate table. A schematic drawing is shown in figure 1. As we modified a conventional sputtering machine, the two targets were attached onto the single cathode. To avoid intermixing of the fluxes, shields (the vertical plates) and a mask (the horizontal plate) were carefully designed and set over the targets. The distance between the plates and the targets were adjusted for the optimum sputtering condition. No contamination by sputtering these plates was observed because they were immediately covered with a thick layer of sputtered atoms. In our case the distance between the plates and the targets is approximately 10 cm. Two semicircular targets 10 cm in diameter were mounted on the water-cooled cathode and sputtered using research-purity argon gas.

The vacuum system was initially pumped down to 2×10^{-6} Torr and the sputtering

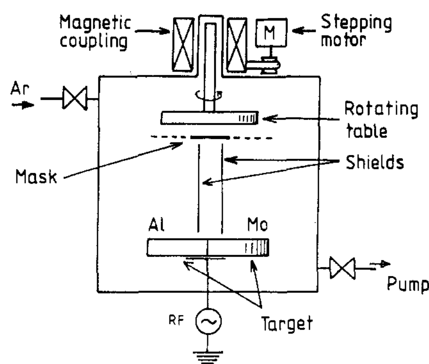

Figure 1. Schematic illustration of the sputtering system for obtaining the multilayers.

was done under a pressure of 5, 10 or 20 × 10^{-3} Torr argon gas. It is generally thought that, under high sputtering gas pressure, many collisions of sputtered atoms with sputtering gas atoms will occur, thereby remarkably decreasing the energies of injecting atoms onto substrates. Accordingly we preferred higher gas pressure and smaller sputtering power when films with small wavelengths were deposited. The substrates used for the studies reported here were glass, Si (1 1 1) and (1 0 0) and Mylar polyimide film, and were initially at room temperature but raised to 100–150 °C during depositions. For the x-ray diffraction intensities, glass substrates were the most desirable, but the films frequently peeled off, and sometimes shattered.

When the mask for 50 at.% films was used, the deposition rate was about 85 Å min^{-1} in 5 × 10^{-3} Torr argon atmosphere (the standard condition) and 50 Å min^{-1} in 1 × 10^{-2} Torr. Except for the samples for transport measurements, Al buffer layers, 1000 Å in thickness, were first deposited without making any significant difference to the crystallography. The total thickness of the CMF film, excluding the buffer layers, was approximately 2.0 or 1.2 μm. Electron microprobe analysis showed a spread in composition within 5 at.%. We deposited a range of periodicities by changing the rotation speed of the substrate table. So the growth rates were all the same for each sputtering condition.

The structure of the CMF was determined by x-ray diffraction, scanning and transmission electron microscopy (SEM, TEM). The x-ray measurements were made using θ–2θ and rocking curve diffraction with Cu Kα radiation. The instrumental resolution was estimated from silicon powder diffraction measurements at 0.02 $Å^{-1}$. All wavelengths were determined by measuring the positions of harmonics around the zero node (the superlattice reflections) and the first and second nodes (the Bragg reflections). They were also calculated using the deposition parameters. In the common region, the layer thickness obtained from both methods agreed well. When no clear harmonics around Bragg peaks could be observed because of the low structural order, we estimated the wavelength by the latter method. The full width at half-maximum (FWHM) of the rocking curve of the first Bragg (central) peak was taken as a measure of the texture.

The resistivity of the Mo/Al CMF was determined by four-point resistance measurements of the samples, which had silicon substrates and no buffer layers. The conduction channel had the approximate dimensions 10 mm × 5 mm × 2 μm and the current was typically of the order of 1 mA. A temperature-controlled cooling system permitted measurement from 4 to 300 K. All the resistivities were those parallel to the films. The current–voltage characteristics were also investigated at room temperature and 77 K.

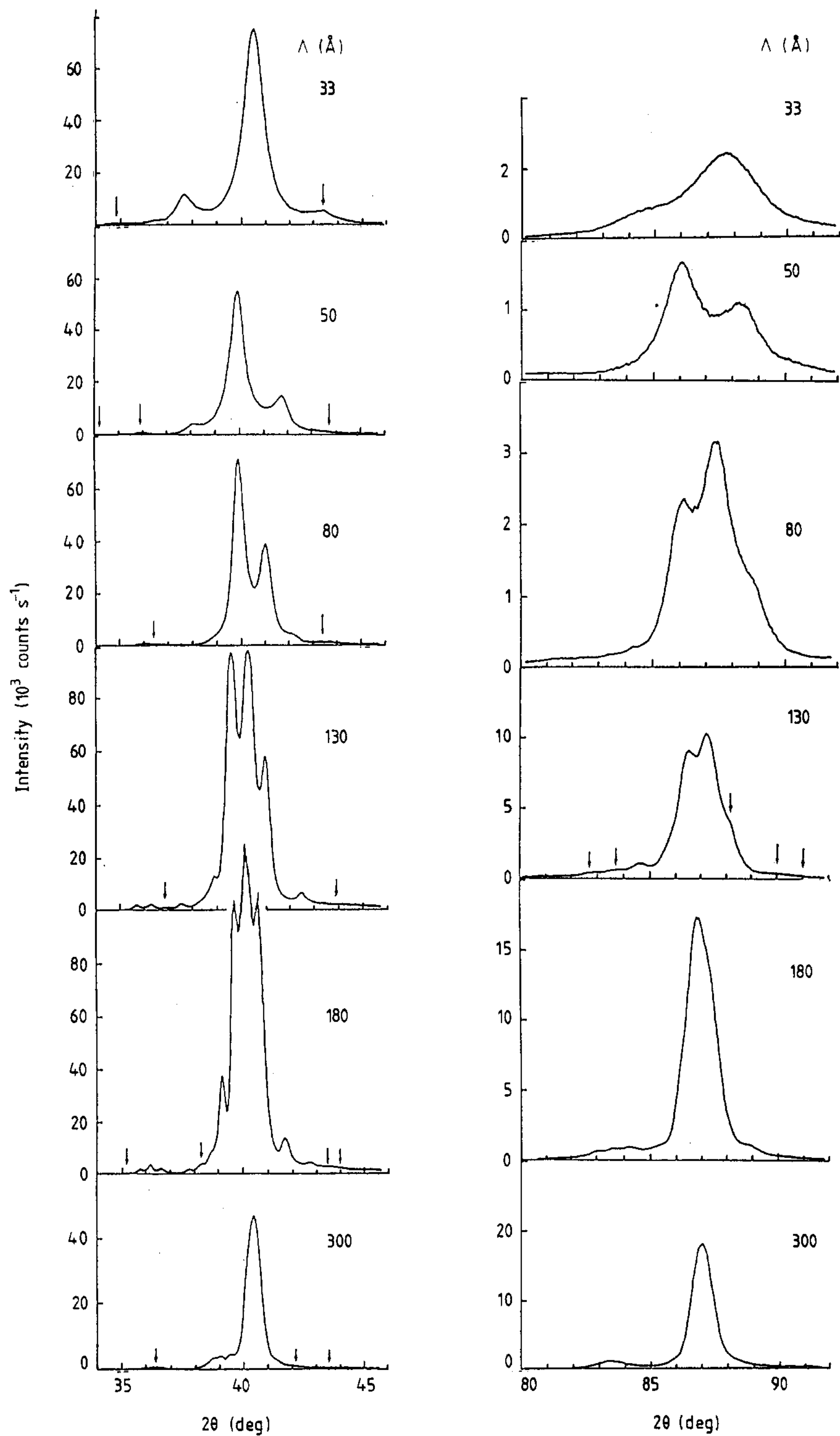

Figure 2. X-ray θ–2θ diffraction patterns around the first Bragg peaks for the 1:1 films sputtered under the standard Ar pressure.

3. Structure of Mo/Al multilayers

First, the standard x-ray diffraction method was used to determine modulation wavelengths and structures. Figure 2 shows the x-ray intensities obtained for Mo : Al = 1 : 1 samples examined in the θ–2θ reflection geometry. For all wavelengths strong and sharp Bragg peaks with first-order and higher-order satellites can be recognised around both the first and the second nodes. No other Bragg peaks except these were observed. For $\Lambda > 200$ Å the peaks are relatively broad and look like two bumps because the satellite peaks cannot be resolved. For lower values of the wavelengths, the diffraction patterns are composed of a sharp central line, namely the Bragg peak, which corresponds to an average inter-atomic spacing, surrounded by the modulation satellites of higher order. In all cases, the reflection from the buffer layer was negligible.

For 200 Å $> \Lambda >$ 60 Å the peaks are reasonably sharp, indicating good crystallisation perpendicular to the films, whereas with decreasing wavelength these peaks become relatively broad and small. In order to synthesise films with $\Lambda < 40$ Å the standard sputtering condition was not suitable. When the sputtering was performed under higher argon gas pressure, we were able to obtain films with smaller, 40 Å $> \Lambda >$ 15 Å, wavelengths. This improvement was more noticeable for films with 1 : 1 composition than for Mo : Al = 1 : 3 films, suggesting that structural disordering is taking place mainly in the aluminium layers. Figure 3 shows the intensities for the films prepared under the pressure of 1×10^{-2} Torr (compare 34 Å in figure 3 with 33 Å in figure 2). The peaks are very sharp and reasonably intense, as expected, but still higher pressures did not give further improvements. Below 20 Å clear satellites were no longer visible, but the superlattice reflections were still resolvable, and the central peaks were still very sharp. The high Ar pressure condition was less suitable for large wavelengths and inadequate above 70 Å.

Below 15 Å even the central peaks became diffuse and we can conclude that a crystalline Mo/Al CMF with $\Lambda <$ 15 Å cannot be prepared by the method described here. A film designated $\Lambda <$ 15 Å is merely a compositionally modulated film with a sinusoidal modulation profile. If films with much smaller wavelengths are desired, it will be necessary to heat the substrates. Recently, growth of single-crystal CMF by sputtering has been reported (Karkut *et al* 1985, 1986). The temperatures of the substrates were as high as 700 °C. In the case of Mo/Al the difference in the melting points is so large and aluminium is so easily oxidised that we could not find any suitable conditions. Lower Ar pressures did not give any improvement or rather made the sputtering unstable.

For the scattering not along the growth direction, there were broad diffraction rings indicating the samples to consist of small grains with random orientation in the plane. The ω and θ–2θ scans revealed that these films are essentially like fibres showing strong texture in the growth direction, the (110) plane of molybdenum and the (111) plane of aluminium parallel to the substrates, and random grain orientation in the plane. All intensity and pattern observations in the diffraction studies have not changed over a period of years, indicating that no significant diffusion occurs after deposition.

The overall chemical modulation was obtained by measuring the position and intensity of the harmonics around the zero node. The diffraction data on the sample with $\Lambda =$ 146 Å are shown in figure 4. At least 10 harmonics have been observed. For Mo/Al the layer thicknesses of the two metals are nearly the same for films of equal concentration and even-order harmonics are not detectable ideally in this case. In figure 4 the intensities of even harmonics are small compared with those of odd harmonics, indicating that there is merely slight deviation from a square-wave modulation. When the film with 1 : 3

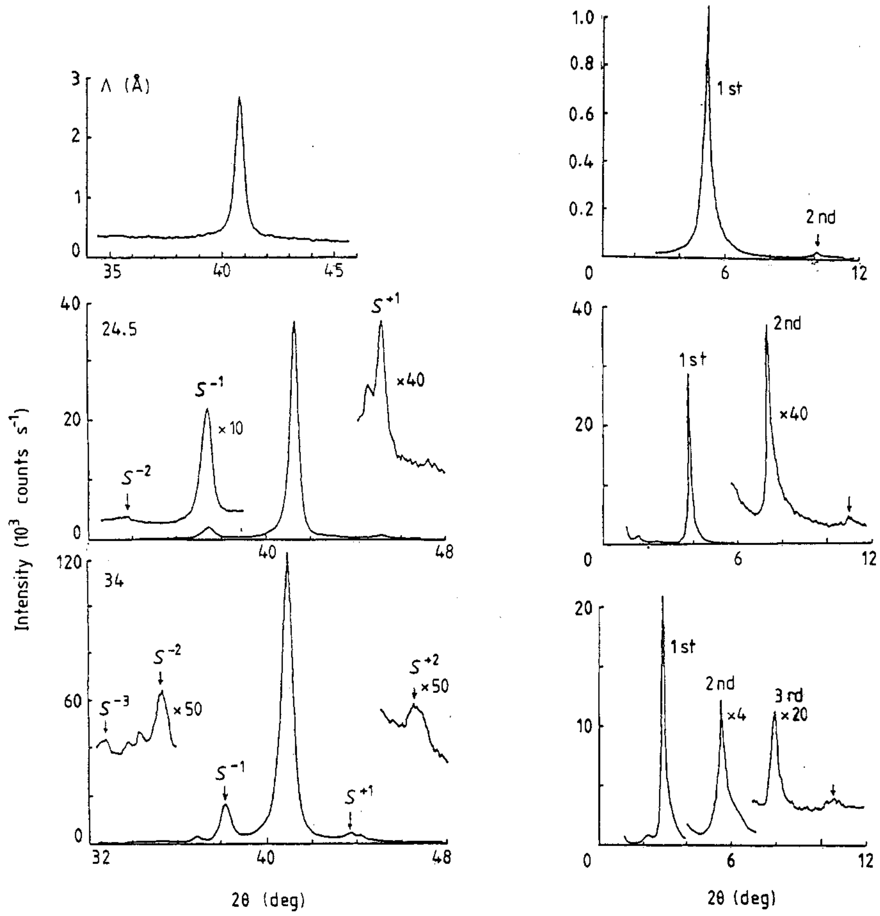

Figure 3. Diffraction patterns for the short-wavelength films with the same composition as figure 2. The films were sputtered under the higher Ar pressure.

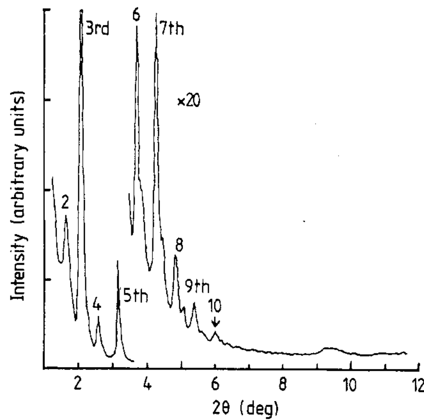

Figure 4. Scan along (000) for the film with the modulation wavelength Λ = 146 Å and 50% aluminium composition, i.e. approximately square-wave modulation. Ideally the even-order harmonics cannot be observed for a symmetrical square wave.

Table 1. The compositional modulation amplitude versus the modulation wavelength less than 60 Å derived from the x-ray intensity ratios.

Wavelength (Å)	21.5	34	42.5	50
A	0.22	0.41	0.34	−0.39

composition was examined, at least 15 harmonics were distinguished. For films with $\Lambda > 250$ Å we could not observe any clear harmonics due to the instrumental resolution.

For a quantitative determination of the chemical modulation, a simple analysis was carried out. In order to obtain the amplitude of compositional modulation A, a harmonic modulation model was employed. In this model

$$C(x) = C_0 + A \sin\left(\frac{2\pi}{\Lambda}x\right) \tag{1}$$

where C_0 is an average and $C(x)$ is the concentration along the x direction. Both the atomic scattering factor f and the inter-planar spacing d vibrate sinusoidally with amplitudes $A\Delta f$ and $d_0\varepsilon$, respectively (Δf is the difference in the atomic scattering factors of the two species, d_0 is an average of the spacings and ε is a strain factor proportional to A). The ratios of the integrated intensities of the satellites to the Bragg peak were derived and after a theoretical correction by some factors described later we determined the amplitude. It is expressed as (Zheng *et al* 1982, Guinier 1963)

$$A = \frac{S^+\sqrt{I^-} - S^-\sqrt{I^+}}{(\Delta f/f_0)S_0} \tag{2}$$

where I^+, I^- are the intensities of the satellites at lower and higher angles integrated by that of the central peak, respectively, S^+, S^- are the scattering vectors of the satellites, S_0 is that of the central peak and f_0 is an average scattering factor of the CMF. The experimental intensities were reduced by the Lorentz, the polarisation and the Debye–Waller factors. The absorpiton factor and the angular dependences of the atomic factors made no difference in this relatively small region.

The modulation amplitudes for small-wavelength films calculated using equation (2) are listed in table 1. For Mo/Al, the heavier element Mo has the smaller inter-atomic spacing with the result that, following the usual notation, the sign of A is always negative, i.e. $I^- < I^+$. For $\Lambda > 60$ Å we were not able to measure the intensity of the first-order satellite at lower angles, because the central peak was extremely high and its background was so intensive as to cover that satellite. We can conclude in such cases that the amplitudes are fairly large and that the signs will be surely negative.

The FWHM and the position of the central peak as functions of the wavelength are shown in figure 5. Considering the instrumental resolution, the peaks are reasonably sharp for films with large wavelengths. With decreasing wavelength in the region less than 60 Å, the FWHM begins to increase, reaching maximum at approximately 40 Å. Afterwards it decreases rather rapidly, and below 30 Å it has approached a constant value again. The change of the peak position behaves in a similar way to the FWHM, i.e. it starts to increase at 60 Å (indicating a smaller average inter-atomic spacing) and becomes constant below 40 Å. All the positions shifted to higher angles than expected from the weighted mean of the corresponding bulk materials. If films expand in the plane on average, in contrast compressive strains will remain in the growth direction.

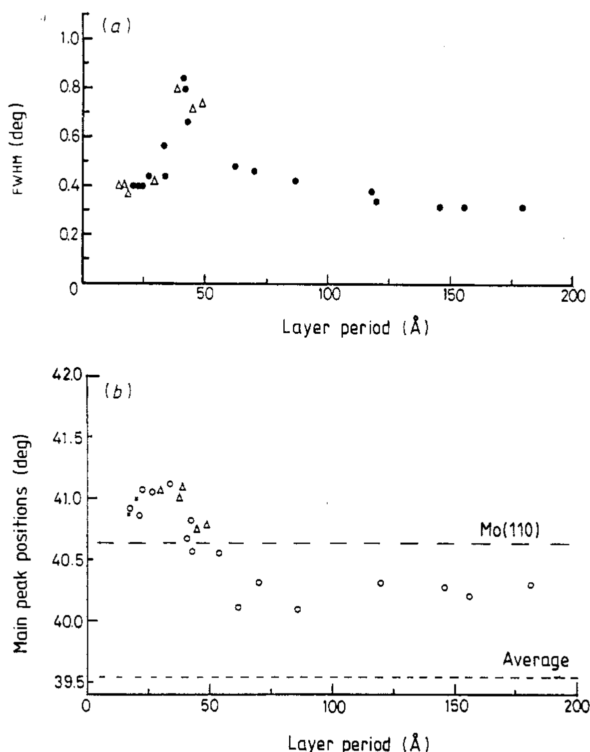

Figure 5. (*a*) FWHM and (*b*) the position of the central peak as functions of the wavelength, for 1 : 1 Mo : Al films. The instrumental resolution is about 0.3° and there is no correction for it.

This can describe very well the cause of the shift of the positions of the Bragg peaks. It is a fact that residual strain becomes excessive at a film thickness above about 2.0 μm and that we can easily observe curvature of thin substrates.

We could not conclude to which type of broadening the FWHM of Mo/Al belongs, Δq = constant or $\Delta q/q$ = constant. One possible reason for the broadening is the decrease of grain size, but it seems unlikely that the size should increase again with decreasing wavelength in the region less than 40 Å. Fluctuation of the wavelength is less probable (Carcia and Suna 1983) because the fluctuation of each deposition rate should be constant for all wavelengths and its effect as a function of wavelength should be more pronounced at smaller wavelengths. The main reason is probably misfit dislocations, and accordingly the interfaces of the small-wavelength films are at least partially coherent (McWhan *et al* 1983). Taking the large strains into account, it is qualitatively possible to explain the intensity inversion of the x-ray satellites ($I^- > I^+$), which occurs when $\Lambda < 40$ Å.

In order to make a more realistic scheme of the structure and to analyse the manifolds shown in figures 2 and 3, computer programs were written to calculate the intensity as a function of scattering along the growth direction (θ–2θ). In a previous analysis we attributed what determines the width of the peaks to the correlation length of the polycrystalline films, which is in a sense the grain size. This may hold generally, but for multilayers it is not the only predominant factor that determines the Bragg peak width, especially in the small-wavelength region ($\Lambda < 60$ Å).

In the present paper we took account of the wavelength fluctuation effect on the x-ray diffraction patterns. The model is based on the theory for paracrystalline materials (see e.g. Cowley 1981). This assumes alternating layers of Mo and Al, or mixed layers (diffused region). The peak intensity has been calculated as

$$I(q) = \left|\sum f_n \exp(\mathrm{i}qx_n)\right|^2 \tag{3}$$

where $q = (4\pi/\lambda)\sin\theta$, q is the x component of the scattering vector (parallel to the growth direction), θ is the diffraction angle, λ is the wavelength of the x-rays, x_n is the position of the nth plane (perpendicular to the x direction) and f_n = (atomic scattering factor) × (density of atoms in the plane) × (the Debye–Waller factor) of the nth plane. To compare with experimental spectra, $I(q)$ was reduced by some factors described already (Lorentz and polarisation). Also q was scanned around $q_j = (2\pi/d_0)j$, $j = 0, 1, 2, 3$, where d_0 is the average inter-atomic spacing.

If the distribution of Λ is a Gaussian distribution with average $\bar{\Lambda}$ and standard deviation σ, which deviates from the usual distribution in the statistics by a factor of $\sqrt{2}$, then

$$I(q) = \frac{1 + \exp(-Nq^2\sigma^2/2) - 2\exp(-Nq^2\sigma^2/4)\cos(N\bar{\Lambda}q)}{1 + \exp(-q^2\sigma^2/2) - 2\exp(-q^2\sigma^2/4)\cos(\bar{\Lambda}q)}|F(q)|^2$$
$$= L(N, q)|F(q)|^2 \tag{4}$$

where N is the total number for the unit structure. The first factor is written as an extended Laue function, $L(N, q)$ (Clemens and Gay 1987, Fujii *et al* 1986, Sevenhans *et al* 1986), and the second factor is an average crystal structure factor for the unit written here as $F(q)$. Considering a multilayer to consist of a material with scattering power f and inter-planar spacing d followed by negligibly low scattering region, $F(q)$ is very simple. When each region has its own scattering power, the fluctuation of Λ is divided into fluctuations of the scattering structures (Mo layer and Al layer) in each unit cell and $F(q)$ becomes very complicated.

In order to calculate $F(q)$, two types of unit structure were employed. The first model used was the well known step model, and the second, which we name the trapezoidal model, assumes linear compositionally grading regions at the interfaces. Of course the compositional modulation is accompanied by those of the inter-atomic spacing and the scattering power. For the step model, $F(q)$ is expressed as a sum of Laue functions multiplied by Debye–Waller-like factors.

Figure 6 shows the x-ray diffraction patterns for wavelengths of 50, 85, 170 and 330 Å calculated using simple trapezoidal models, which are to be compared with figures 2 and 3. In the calculations we assumed the number of planes in the compositionally grading region $NI = 5$. This number does not play a key role in the diffraction pattern determination. Except for the intensity decreasing rates of the satellites with order, there was no significant difference between the step and trapezoidal models. The fluctuation effect was checked using the step model and the trapezoidal model in which a composition-weighted fluctuation effect was assumed, but no special effect was found. The disadvantage of the no-fluctuation theory is that we must accept a correlation length that is an integer multiple of the wavelength, which causes a rather rough change of the pattern on changing N. The fluctuation theory is free from this disadvantage and changes patterns smoothly. The fluctuation of the number of planes in each region was estimated at 0.35 for all wavelengths treated here.

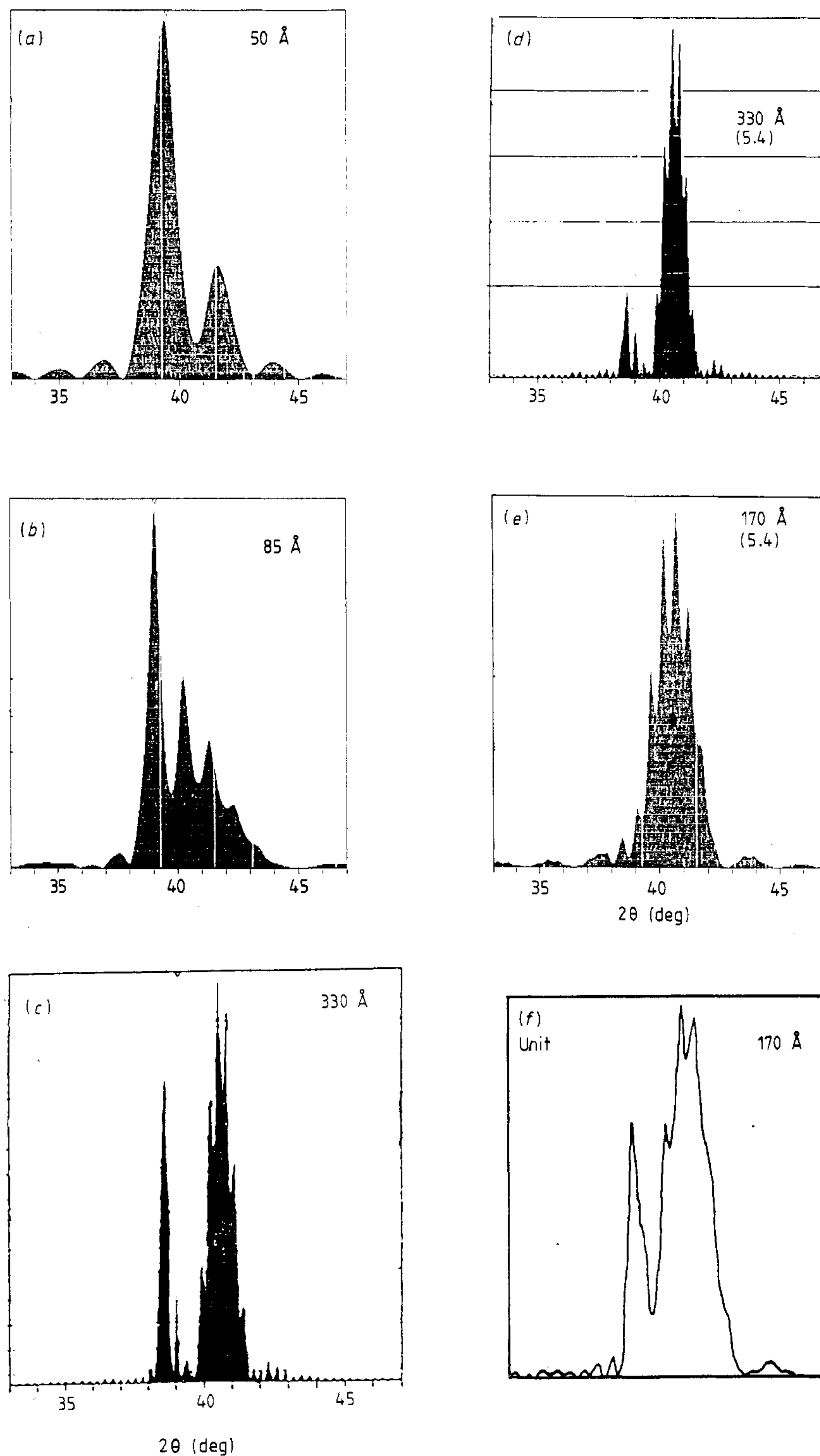

Figure 6. (*a*)–(*e*) Calculated diffraction patterns considering the fluctuation effect with trapezoidal modulation waves and (*f*) the x-ray crystal structure factor of the unit for $\Lambda = 170$ Å.

For $\Lambda > 150$ Å there was an unexpected serious deviation from the experiments. The calculated intensities of the low-angle satellites were rather large, which should be attributed to diffraction from the aluminium layers. In order to correct the calculated values, the ratio of atomic scattering powers must be changed (fixing that of Mo and changing that of Al). No parameters in equation (3) can rectify the deviations except for this ratio. Adjusting the intensities of the low-angle peaks for $\Lambda = 330$ Å (figures 6(*d*) and (*e*)), we obtained the value of Al atomic scattering factor 5.4 (if that of Mo = 42), which also gave a remarkable improvement of the pattern for $\Lambda = 170$ Å. Without this correction the intensities are always nearly equal using equation (3) type theory, and such a case is more invalid when the wavelength approaches the film thickness. We think the reduction is not the change of scattering powers of individual atoms but that of individual layers. Since the correction was more necessary for films with large wavelengths, this reduction of the atomic scattering power should correspond to loss of perfection of parallel layer stacking rather than loss of short-range order in the grain.

In order to explain the satellite intensity inversion for $\Lambda < 40$ Å, three-step models were employed, which take account of some kinds of compound layers, such as Al_3Mo and Mo_3Al, at interfaces. However, these compound layer models proved to be wide of the mark. The reason for this failure is that the scattering power of compound layers is always intermediate and that the more the compound layers are formed the more pure Al and Mo layers decrease.

In summary, we have calculated the x-ray diffraction patterns using the step and trapezoidal models taking account of the wavelength fluctuation. We found a rather rapid decrease of the satellite intensities as a function of their orders in the trapezoidal model. The fluctuation of the wavelength was evaluated at 0.35 throughout all wavelengths, which is reasonable if the fluctuation of the wavelength is caused by the fluctuations of the deposition rates. In the large-wavelength region the crystal structural factor of the unit already contains the Laue functions, as the unit contains many atomic planes already, and the functions have sharp peaks and determine the outline of the diffraction patterns (figure 6(*f*)). We are now able to conclude that for the small-wavelength region the patterns are determined by inter-diffusion and for the large-wavelength region by atomic plane stacking, inter-spacing and parallelism between planes, in the unit structure, which is less important in the former case. We emphasise that no intensity inversion occurs by insertion of any kind of compound layer.

4. Transport properties

Figure 7 shows a graph of the resistivity (4.2 and 280 K) versus the inverse modulation wavelength for a series of Mo/Al samples with a 1:1 composition. For wavelength above 60 Å the intensity is approximately inversely proportional to the individual layer thickness, as predicted for the wavelength-limited mean free path, and the TCR are positive in sign. In this wavelength region all the resistivities saturated by the residual below 50 K showing that the films are quite disordered compared with the bulk materials. The typical resistivity ratio, $\rho(280\ \mathrm{K})/\rho(4.2\ \mathrm{K})$, was about 1.2 and not as small as for metallic multilayers. On decreasing the wavelength down to 60 Å, no saturation but a negative resistivity gradient with respect to the temperature was observed, where the resistivity was 100–150 $\mu\Omega$ cm.

Figure 8 shows the gradients of the resistivity versus temperature curves as a function of wavelength. When they are divided by the resistivities $(1/\rho)(\mathrm{d}\rho/\mathrm{d}T)$ they get close

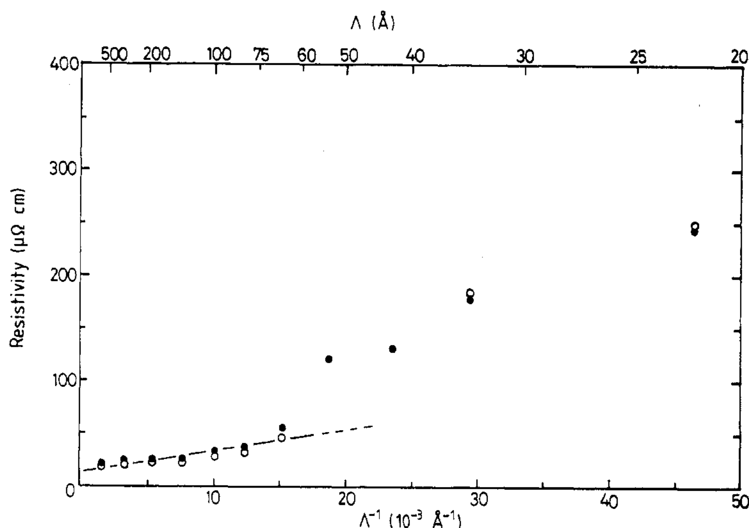

Figure 7. Electrical resistivity at 280 (●) and 4.2 K (○) as a function of inverse wavelength for a series of Mo/Al with 50% aluminium composition.

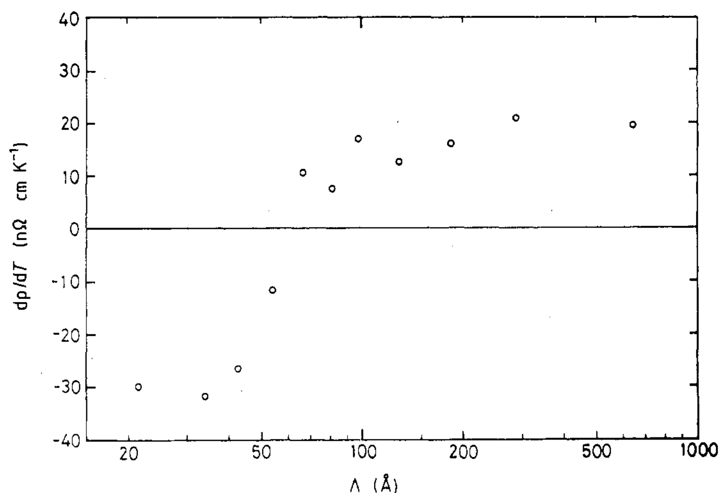

Figure 8. Temperature gradient of the resistivities versus the wavelengths.

to the horizontal line (TCR = 0) from the negative side, because the resistivity itself becomes progressively larger with decreasing wavelength. The TCR shows a rather sudden change from positive to negative values as a function of wavelength. It changes sign where the broadening and shift of the Bragg peak occur.

The origin of the high resistivity, especially when surpassing the expected value from the linear dependence in figure 7, and of the non-metallic behaviour at small wavelengths should be explained theoretically. Here we offer an explanation using the resistivity theory by Dimmich (1985). This theory is based on an interfacial scattering like Fuchs',

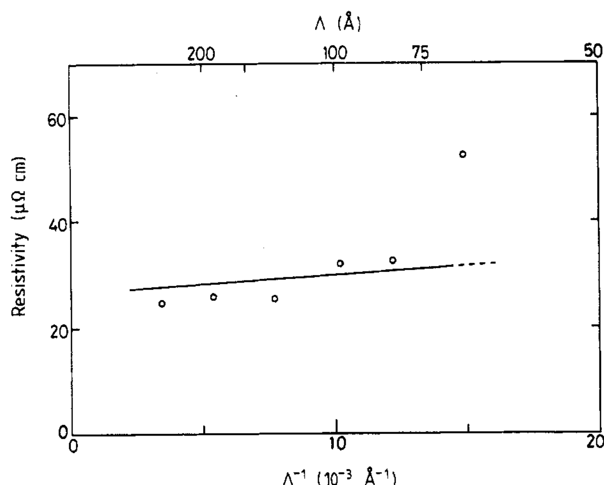

Figure 9. Calculated resistivities at 273 K using temperature-independent parameters $p = 0$, $R = 0.67$ and $b_1 = b_2 = 65$ Å for films with positive TCR.

and grain boundary scattering of polycrystalline films like Mayadas–Stokes (Mayadas and Shatzkes 1970). It allows a finite probability p of coherent passage of an electron across an interface and assumes a reflection coefficient R for an electron striking a grain boundary in the metal layer with an average distance $\bar{b}$. All the temperature dependences follow from the temperature dependence of the mean free paths of the electrons. Consequently, this dependence plays the key role in TCR. Besides the probability and the reflection coefficient, geometrical parameters, such as layer thicknesses d_1 and d_2, average grain sizes b_1 and b_2, and base resistivities are to be set. In Dimmich's calculation, infinitely thick films and bulk resistivities were basic requisites, but we do not have to obey the latter limitation.

The results are shown in figure 9, for which temperature- and wavelength-independent R and p and the bulk resistivities and mean free paths were used. High reflection coefficients and low probabilities of coherent passage were indispensable to explain the high resistivities in figure 7. If the base resistivities were not those of the bulk, but were treated as variable parameters, a closer fit could be performed. Except for the large deviation at $\Lambda = 65$ Å where the TCR is nearly zero, the agreement is not worse and is better for $\Lambda > 150$ Å with a smaller R and a larger p. The most uncertain geometrical parameter $\bar{b}$ (common to both layers for simplicity) is the most dominant one in our calculation and still more dominant at lower temperatures. Mayadas and Shatzkes (1970) assumed $\bar{b}$ to be equal to the film thickness and believed $0 < R < 0.3$ to be reasonable. In the region from 250 down to 80 Å a constant grain size model calculation with the parameters $p = 0$, $R = 0.67$ and $\bar{b} = 65$ Å was most preferable and a change of p made only a trivial difference, as expected.

The facts that a high boundary scattering coefficient and an extremely small grain size are indispensable for a reasonable fitting means that the key factor is not the roughness of the interfaces, namely coherent passage across interfaces, but grain boundary scattering. Even with the grain scattering model, the grain size and the reflection coefficient are too large, which suggests a more or less short-range disordering of the crystal structure. At this stage it is impossible to take account of the disordering effect.

TCR were also calculated using the same parameters taking account of the temperature dependences of the bulk mean free paths for the films with evidently positive TCR. When $\Lambda = 130$ Å, the calculated TCR $= 6.2 \times 10^{-4}\,\mathrm{K}^{-1}$, which is to be compared with the experimental value $5 \times 10^{-4}\,\mathrm{K}^{-1}$. Generally, the higher the resistivity, the smaller is the TCR, and negative TCR are usual for high-resistivity materials. This behaviour is more emphasised in metallic amorphous materials. In our calculations with temperature-independent parameters, no negative TCR were derived.

When the resistivity of a metal is considered, it is usually divided into different contributions according to Matthiessen's rule, just like scattering due to an ideal lattice, impurities and structural imperfections. The latter two are thought to be temperature-independent in metals. In our consideration the last one was divided into two contributions, moreover. The first part consists of the interface or surface scattering and the grain boundary scattering (the geometrical scatterings), and the second consists of the rest. Now let the intrinsic scattering be composed of the lattice scattering and scatterings due to all structural imperfections except the geometrical. Here we describe the resistivity as follows (this picture becomes invalid with increase of resistivity of metals but still useful when TCR $\geqslant 0$):

$$\rho = \rho_{\mathrm{int}} + \rho_{\mathrm{imp}} + \rho_{\mathrm{gmt}} \tag{5}$$

where int represents intrinsic scattering, imp impurity scattering and gmt the two geometrical scatterings. If the intrinsic scattering is controlled by phonon scattering characteristic of bulk metals and the impurity scattering is almost temperature-independent, no change of the sign of TCR took place. There the geometrical scatterings could only suppress the temperature gradients, especially at low temperature. In order to derive a negative TCR, p and R should decrease, or the intrinsic scattering should decrease with increasing temperature, which is quite different from the crystalline metal lattice scatterings.

It is generally known that, when an extremely thin film less than 100 Å in thickness is deposited, the film consists of many islands or coalescences of them (a network structure), and the resistivity increases progressively with decreasing film thickness. This structure may change the intrinsic scatterings remarkably, and at least the geometrical scatterings are seriously affected. For these films, thermally activated and non-ohmic conductions are always recognised. As a multilayer film is an assembly of extremely thin layers, it is natural that the film should be a network film and its TCR be negative. In order to check the conduction behaviours of negative TCR films we measured the I–V (current–voltage) characteristics at low temperature. Contrary to our expectation, only ohmic behaviours were verified even for the perfectly negative TCR regime in figure 8.

One cross-sectional view by TEM is shown in figure 10, where the wavelength is 33 Å and the TCR is undoubtedly much less than zero. The direct observation shows that the size of the crystal grains is not small and that the grains are highly oriented (Ichinose *et al* 1988). Patches of coherent regions extending over many layers and interfaces are observed and no network structure can be recognised, though slightly wavy interfaces do occur. Furthermore the inter-atomic spacings are nearly the same as indicated by the x-ray diffraction studies ($d_{\mathrm{Mo}}(1\,1\,0) = d_{\mathrm{Al}}(1\,1\,1)$). These facts argue against the extremely small grain size and the consequent large reflection coefficient in our resistivity calculations. It is an obvious aim of future investigations to explain the cause of the coherent interfaces despite the structurally dissimilar metals.

Nb/Cu is the most precisely investigated CMF regarding transport properties. Here negative TCR conduction is explained by localisation-type theories, electron localisation

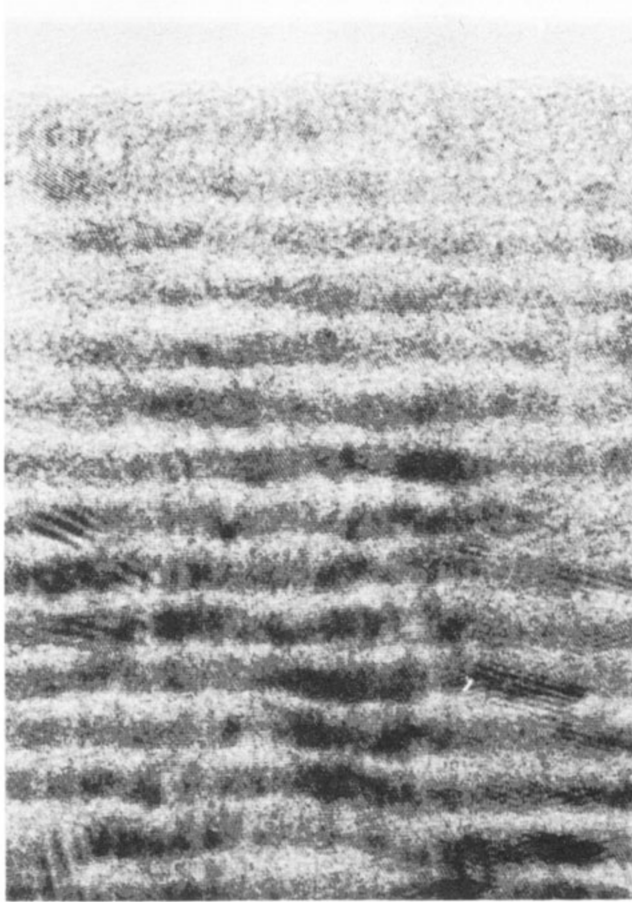

Figure 10. Lattice image of Mo/Al viewed in the direction perpendicular to the film. The interfaces prove to be smooth and ordered irrespective of each layer being extremely thin.

effects and/or electron–electron interaction effects (Werner *et al* 1982). Another CMF that shows clear negative TCR at small wavelengths is Mo/Ni (Khan *et al* 1983), where the change of the electron conduction behaviour is believed to be due to the structural changes that were indicated by surface-phonon studies. In Al/Ge, the other case, the resistivity increases extraordinarily with decreasing wavelength down to 160 Å (Haywood and Ast 1978) and presumably a negative TCR would be observed (there were no TCR data in their paper). The situation was quite different from those of two previous metallic CMF and Mo/Al since Al/Ge shows negative TCR because of obvious network structure, which was suggested by electron microscope studies.

Now we should stress that there are neither network structure, compound layers nor insulating layers in Mo/Al. Impurity is one of the most likely reasons for high resistivities at short wavelengths. As the growth rates were constant for the same sputtering conditions, the concentrations of impurities should be almost the same. For films with Λ = 40–60 Å the resistivities of the standard condition (high growth rate) are a little larger than those prepared under the higher Ar pressure, and the deviation in figure 7

is already obvious at 70 Å (standard condition). So we think impurity is probably less important. Furthermore, impurity cannot usually change the sign of TCR. The TEM images denied obvious compound (oxidised) regions. With decreasing wavelength structural changes occur, which change the electronic structures and sometimes make TCR negative. At this stage what can be said is that the conduction behaviour is intimately concerned with the gradual disordering indicated by the diffraction studies. The behaviour in the non-metallic regime is quite like those of amorphous materials.

Furthermore, we observed increases of superconducting transition temperature. Molybdenum and aluminium are superconducting metals with low transition temperatures, 0.92 and 1.2 K, respectively. Geerk *et al* (1982) studied the superconducting properties of Mo/Al as well as Nb/Al and obtained the temperature 3.1 K for Mo/Al (Λ = 40 Å) and 2.9 K for Nb/Al (Λ = 24 Å). The latter is too low for a proximity effect because the temperature of bulk niobium is as high as 9.3 K. It is closer to the transition temperature of amorphous niobium. Like niobium films, highly resistive molybdenum and aluminium films have enhanced transition temperatures around 9 K and between 2 and 5 K, respectively (Collver and Hammond 1973, Strongin and Kammerer 1968). The transition temperatures were no less than 3.5 K for our Mo/Al with $\Lambda < 70$ Å. Perhaps the main reason for this enhancement is neither the superlattice structures, which affect the band structure, nor the inter-diffusion, but the short mean free paths in the films. The resistivities of single-component molybdenum and aluminium films prepared under various sputtering conditions were also measured, and occasionally transition temperatures as high as 7 K were observed for comparatively resistive molybdenum films. For large wavelengths they were less than 3 K, as expected for many other CMF.

5. Conclusions

We have shown that fine Mo/Al CMF can be fabricated even by a simple multi-target sputtering apparatus. The structure of the films were highly textured with manifolds of x-ray diffraction patterns. The calculations of the patterns indicated that inter-diffusion determines the diffraction patterns in the small-wavelength region and that the crystal structure factor of the unit structure does so in the large-wavelength region. All the diffraction studies showed the existence of a structural transition region between 40 and 60 Å and that the interfaces are partially coherent. The resistivity increased remarkably with decreasing modulation wavelengths in the region less than 60 Å. Negative TCR were found for small wavelengths but no network structure was observed. It may be better to discuss the origin of negative TCR as conduction in disordered materials. This will be the subject of further theoretical investigations.

Acknowledgments

One of the authors (TH) is greatly indebted to Dr H Ichinose and Professor Y Ishida (Institute of Industrial Science, University of Tokyo) for the TEM observations and would like to thank Professor M Doyama (Nagoya University) for his constant encouragement. Special thanks are also due to Dr H Jorgensen and T Sasaki for stimulating discussions and assistance, and finally to Dr M Imafuku for the chance to start this work.

References

Banerjee I and Schuller I K 1984 *J. Low Temp. Phys.* **54** 501
Banerjee I, Yang Q S, Falco C M and Schuller I K 1982 *Solid State Commun.* **41** 805
Carcia P F and Suna A 1983 *J. Appl. Phys.* **54** 2000
Carcia P F, Suna A, Onn D G and van Antwerp R 1985 *Superlatt. Microstruct.* **1** 101
Clarke R, Morelli D, Uher C, Homma H and Schuller I K 1985 *Superlatt. Microstruct.* **1** 125
Clemens B M and Gay J G 1987 *Phys. Rev.* B **35** 9337
Collver M M and Hammond R H 1973 *Phys. Rev. Lett.* **30** 92
Cowley J M 1981 *Diffraction Physics* (Amsterdam: North-Holland) ch 7
Dimmich R 1985 *J. Phys. F: Met. Phys.* **15** 2477
Flevaris N K, Ketterson J B and Hilliard J E 1982 *J. Appl. Phys.* **53** 8046
Fujii Y, Ohnishi T, Ishihara T, Yamada Y, Kawaguchi K, Nakayama N and Shinjo T 1986 *J. Phys. Soc. Japan* **55** 251
Geerk J, Gurvitch M, McWhan D B and Rowell J M 1982 *Physica* **109 & 110B** 1775
Guinier A 1963 *X-ray Diffraction in Crystals, Imperfect Crystals and Amorphous Bodies* (San Francisco: Freeman) ch 13
Gurvitch M 1986 *Phys. Rev.* B **34** 540
Gyorgy E M, McWhan D B, Dillon J F Jr, Walker L R and Waszcak J V 1982 *Phys. Rev.* B **25** 6739
Gyorgy E M, McWhan D B, Dillon J F Jr, Walker L R, Waszcak J V, Musser D P and Willens R H 1983 *J. Magn. Magn. Mater.* **31–34** 915
Haywood T W and Ast D G 1978 *Phys. Rev.* B **18** 2225
Ichinose H, Ishida Y, Izumiya T and Yamamoto R 1988 *MRS Meeting on Advanced Materials (Tokyo), Proc. Multilayer Symp.* vol 10 ed K Yamamoto and T Ohno p 533
Kaneko T, Sasaki T, Sakuda M, Yamamoto R, Nakamura T, Yamamoto H and Tanaka S 1988 *J. Phys. F: Met. Phys.* **18** 2053
Karkut M G, Ariosa D, Triscone J M and Fischer O 1985 *Phys. Rev.* B **32** 4800
Karkut M G, Triscone J M, Ariosa D and Fischer O 1986 *Phys. Rev.* B **34** 1986
Khan M R, Chun C S L, Felcher G P, Grimsditch M, Kueny A, Falco C M and Schuller I K 1983 *Phys. Rev.* B **27** 7186
Lowe W P, Barbee T W Jr, Geball T H and McWhan D B 1981 *Phys. Rev.* B **24** 6139
Lowe W P and Geball T H 1984 *Phys. Rev.* B **29** 4961
McWhan D B, Gurvitch M, Rowell J M and Walker L R 1983 *J. Appl. Phys.* **54** 3886
Mayadas A F and Shatzkes M 1970 *Phys. Rev.* B **1** 1382
Qian Y J, Zheng J Q, Sarma B K, Yang H Q, Ketterson J B and Hilliard J E 1982 *J. Low Temp. Phys.* **49** 279
Sasaki T, Kaneko T, Sakuda M and Yamamoto R 1988 *J. Phys. F: Met. Phys.* **18** L113
Schuller I K, Falco C M, Hilliard J E, Ketterson J B, Thaler B J, Lacoe R and Dee R 1979 *Modulated Structures 1979* ed J M Cowley *et al* (New York: American Institute of Physics) p 417
Sevenhans W, Gijs M, Bruynseraede, Homma H and Schuller I K 1986 *Phys. Rev.* B **34** 5955
Shiroishi Y, Sellers C, Hilliard J E and Ketterson J B 1987 *J. Appl. Phys.* **62** 3694
Slaughter J, Bass J, Pratt W P Jr, Schroeder P A and Sato H 1987 *Proc. 18th Int. Conf. Low Temp. Phys. (Kyoto); Japan. J. Appl. Phys.* **26** Suppl 26–3, 1451
Strongin M and Kammerer O F 1968 *J. Appl. Phys.* **35** 2505
Thaler B J, Ketterson J B and Hilliard J E 1978 *Phys. Rev. Lett.* **41** 336
Uher C, Clarke R, Zheng G-G and Schuller I K 1984 *Phys. Rev.* B **30** 453
Werner T R, Banerjee I, Yang Q S, Falco C M and Schuller I K 1982 *Phys. Rev.* B **26** 2224
Zheng J Q, Falco C M, Ketterson J B and Schuller I K 1981a *Appl. Phys. Lett.* **38** 424
Zheng J Q, Ketterson J B, Falco C M and Schuller I K 1981b *Physica* **108B** 945
—— 1982 *J. Appl. Phys.* **53** 3150